A Metal–Organic-Framework-Based Electrolyte with Nanowetted Interfaces for High-Energy-Density Solid-State Lithium Battery

*Ziqi Wang, Rui Tan, Hongbin Wang, Luyi Yang, Jiangtao Hu, Haibiao Chen, and Feng Pan**

Solid-state batteries (SSBs) are promising for safer energy storage, but their active loading and energy density have been limited by large interfacial impedance caused by the poor Li^+ transport kinetics between the solid-state electrolyte and the electrode materials. To address the interfacial issue and achieve higher energy density, herein, a novel solid-like electrolyte (SLE) based on ionic-liquid-impregnated metal–organic framework nanocrystals (Li-IL@MOF) is reported, which demonstrates excellent electrochemical properties, including a high room-temperature ionic conductivity of 3.0×10^{-4} S cm^{-1}, an improved Li^+ transference number of 0.36, and good compatibilities against both Li metal and active electrodes with low interfacial resistances. The Li-IL@MOF SLE is further integrated into a rechargeable Li|$LiFePO_4$ SSB with an unprecedented active loading of 25 mg cm^{-2}, and the battery exhibits remarkable performance over a wide temperature range from −20 up to 150 °C. Besides the intrinsically high ionic conductivity of Li-IL@MOF, the unique interfacial contact between the SLE and the active electrodes owing to an interfacial wettability effect of the nanoconfined Li-IL guests, which creates an effective 3D Li^+ conductive network throughout the whole battery, is considered to be the key factor for the excellent performance of the SSB.

Lithium solid-state battery (SSB) has been considered as a promising candidate for the next-generation energy storage as it can avoid the potential risks of volatilization, leakage, and fire, which often happen to the conventional Li-ion batteries with liquid-type electrolytes.[1,2] Moreover, benefiting from the intrinsic solid characteristic of the solid-state electrolyte (SSE), Li dendrite growth can be suppressed, thus directly employing Li metal as the anode to achieve a higher energy density becomes possible.[3,4] The major fundamental issue obstructing the practical applications of SSBs is the large interfacial resistance caused by the poor physical contact between the SSEs and the electrode materials.[5,6] The solid–solid hard contact substantially limits the overall Li^+ transport, and an adequate electrochemical activity is achieved only with limited loading of active materials and energy density of SSBs.[7,8] Therefore, developing an optimized SSE with the advantages of liquid electrolytes which can be highly conductive for ions both in the bulk phase and at the contact interfaces is essential for the broad applications of SSBs.

To this end, in this Communication we propose a novel solid-like electrolyte (SLE, Li-IL@MOF) based on a metal–organic framework (MOF) and a Li^+ containing ionic liquid (Li-IL), in which the porous MOF host provides a stable 3D open solid framework and the Li-IL guest serves as the Li^+ conductor. The Li-IL encapsulated in the MOF lattice loses its primitive liquid characteristics including the "free-flowing" behavior but preserves the high ionic conductivity. Distinguished from the conventional SSEs with solid–solid hard contact interfaces, the MOF host featuring a 3D open framework provides many direct-contact points at atomic level for the active materials with the confined Li-IL, forming abundant nanowetted interfaces to favor the Li^+ transport kinetics. Moreover, the Li-IL@MOF SLE also demonstrated a reasonable electrochemical window, good thermal and mechanical stability, as well as excellent compatibility with Li metal. The Li-IL@MOF SLE was further employed in a $LiFePO_4$ (LFP) solid-state battery using Li metal as the anode and a composite of LFP, Li-IL@MOF and acetylene black as the cathode. Owing to the synergistic effect of a high ionic conductivity and nanowetted interfaces, an effective 3D-connected Li^+ transport network was established throughout the cathode. Even under a very high LFP loading of 25 mg cm^{-2} with a total cathode thickness of 210 μm, the Li|Li-IL@MOF|LFP battery showed remarkable electrochemical properties, such as increased Li^+ transference number of 0.36, a wide operating temperature range (−20 to 150 °C) with good capacity retention, etc. Through the Li-IL@MOF nanocomposite design and the nanowetted interface mechanism, we have demonstrated a feasible approach to develop high energy density SSBs. Although the concept of utilizing Li^+ conductive MOFs as solid-like electrolytes was previously proposed by Long[9] and Kitagawa[10] groups, the practical application of MOF based SLEs in a rechargeable battery system is demonstrated for the first time in this report.

Dr. Z. Wang, R. Tan, Dr. H. Wang, Dr. L. Yang, J. Hu, Prof. H. Chen, Prof. F. Pan
School of Advanced Materials
Peking University Shenzhen Graduate School
Shenzhen 518055, P. R. China
E-mail: panfeng@pkusz.edu.cn

The ORCID identification number(s) for the author(s) of this article can be found under https://doi.org/10.1002/adma.201704436.

DOI: 10.1002/adma.201704436

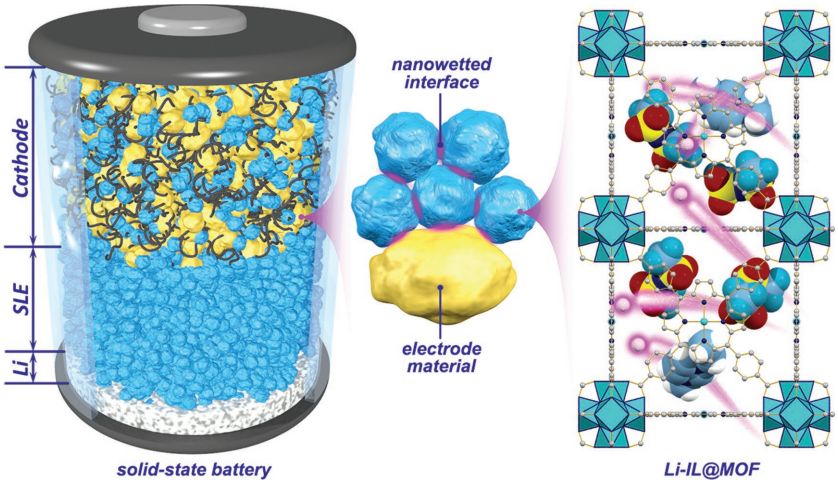

Scheme 1. Schematic illustration for the architecture and nanowetted interfacial mechanism of the solid-state battery with a magnification showing crystal structures of the MOF. $[EMIM]^+$ and $[TFSI]^-$ ions in space-filling model are randomly displayed in the pores of the MOF. The migrating Li^+ ions are highlighted by glowing pink spheres. Hydrogen atoms are omitted in MOF structure for clarity.

A unique solid-state battery system was designed and its working mechanism is illustrated in **Scheme 1**. The ionic liquid we selected is $[EMIM_{0.8}Li_{0.2}][TFSI]$ (about 1 M LiTFSI in [EMIM][TFSI]), where EMIM is 1-ethyl-3-methylimidazolium and TFSI is bis(trifluoromethylsulfonyl)amide. $[EMIM_{0.8}Li_{0.2}]$ [TFSI] is a highly conductive, nonvolatile, and nonflammable electrolyte with low viscosity and acceptable chemical window, and it is commonly used in Li-ion batteries.[11,12] The sizes of $[EMIM]^+$ and $[TFSI]^-$ ions have been calculated to be 7.9 and 7.6 Å, respectively, in the longest dimension.[13] The MOF host material we selected is MOF-525(Cu)[14] which is a highly porous open framework constructed by $Zr_6(IV)O_4(OH)_4$ clusters and [5,10,15,20-tetrakis(4-carboxyphenyl)porphyrin]Cu(II) (CuTCPP) organic linkers, as shown in Scheme 1. The aperture size of MOF-525(Cu) is about 12×7 Å, capable of allowing Li-IL ions to pass through. Such a pore structure can also impose confinement to the internal $[EMIM]^+$ and $[TFSI]^-$ ions, lowering their mobility, and thus increasing the Li^+ transference number. Moreover, MOF-525(Cu) crystals have been proved to be electrochemically stable against Li metal at a high potential,[15] which is essential for electrolyte applications.

The as-synthesized MOF crystals were nearly spherical with a diameter of about 50 nm, as indicated by the scanning electron microscopy (SEM) morphologies (Figure S1a, Supporting Information). X-ray diffraction (XRD) pattern of the as-synthesized MOF is consistent with the simulated one based on reported structure,[14] indicating acceptable phase purity, as shown in Figure S2 (Supporting Information). Occupancy rate of Li-IL ions in the pores of the MOF host directly determines the ionic conductivity of Li-IL@MOF SLE.[10] In order to maximize the Li-IL loading and achieve higher ionic conductivity, the content of Li-IL in the Li-IL@MOF composite was first optimized before other tests. The activated MOF nanocrystals were mixed with different amount of Li-IL and heated under vacuum overnight. Through this process, the residual guest molecules in the MOF crystals were evacuated from the pores for better Li-IL infiltration. The Li-IL@MOF composites were pressed into pellets (Figure S3, Supporting Information) afterward for ionic conductivity determination, which was performed by electrochemical impedance spectroscopy (EIS) with silver-coated stainless steel (SS) electrodes at a temperature ranging from 30 to 100 °C. The Arrhenius plots for the ionic conductivity of Li-IL@MOF SLEs with different Li-IL contents are shown in **Figure 1**a. As can be seen, pristine MOF was close to an insulator, showing a very low intrinsic conductivity. With a fixed mass (1.2 g) of MOF, the ionic conductivity raised with the Li-IL loading amount increasing. Apparently, the ionic conductivity of the composite strongly relies on the conductive paths for the ions, which increase with the concentration of the guest ions in the MOF host.[16] The highest ionic conductivity was observed in the sample with 2.0 mL Li-IL, and the value is close to that of the pristine Li-IL reported previously.[10,17] However, the sample with 2.0 mL Li-IL felt like a wet gel, indicating that the Li-IL could not be absorbed completely by the MOF host. With the Li-IL content less than 1.5 mL, the composites appeared to be "free-flowing" dry powder (see Video S1, Supporting Information), meaning that the Li-IL was completely encapsulated in these samples. X-ray photoelectron spectroscopy (XPS) tests were further carried out on the Li-IL@MOF samples, as shown in Figure S4 (Supporting Information). It should be noted that when excess Li-IL covered the surface of MOF (sample: 2.0 mL Li-IL@1.2 g MOF), the Cu(II) in the MOF ligands could not be detected by XPS. The strong Cu(II) signals observable only in the samples with Li-IL content less than 1.5 mL provided additional proof for complete Li-IL impregnation. Based on the results given above, an optimized ratio (1.5 mL Li-IL@1.2 g MOF, that is, 10.1 wt% LiTFSI, 55.4 wt% [EMIM][TFSI], and 34.5 wt% MOF were contained in the composite) was finally determined and was used in the following studies.

The BET surface area of the MOF nanocrystals was 1630 $m^2 g^{-1}$ and the total pore volume was 1.92 $cm^3 g^{-1}$ according to the N_2 adsorption/desorption isothermal tests (Figure S5a, Supporting Information), confirming the high porosity of MOF host. The BET surface area declined to 21 $m^2 g^{-1}$ (Figure S5b, Supporting Information) and the total pore volume declined to 0.05 $cm^3 g^{-1}$ for Li-IL@MOF composite as a result of the Li-IL impregnation. The significant decrease of the BET surface area and the pore volume indicates that the pores of the MOF have been almost filled by the Li-IL ions. The MOF host appeared to be chemically stable against Li-IL because no significant change in the XRD profiles was observed after Li-IL impregnation, as displayed in Figure S2 (Supporting Information). It is worth noting that the diffraction peaks of the Li-IL@MOF pellet became broad and could not be distinguished at $2\theta > 7°$, indicating that the periodicity of some fine structures within the MOF framework was lost, which we speculate was caused by the inner stress of MOF crystals after mechanical pressing[18,19]

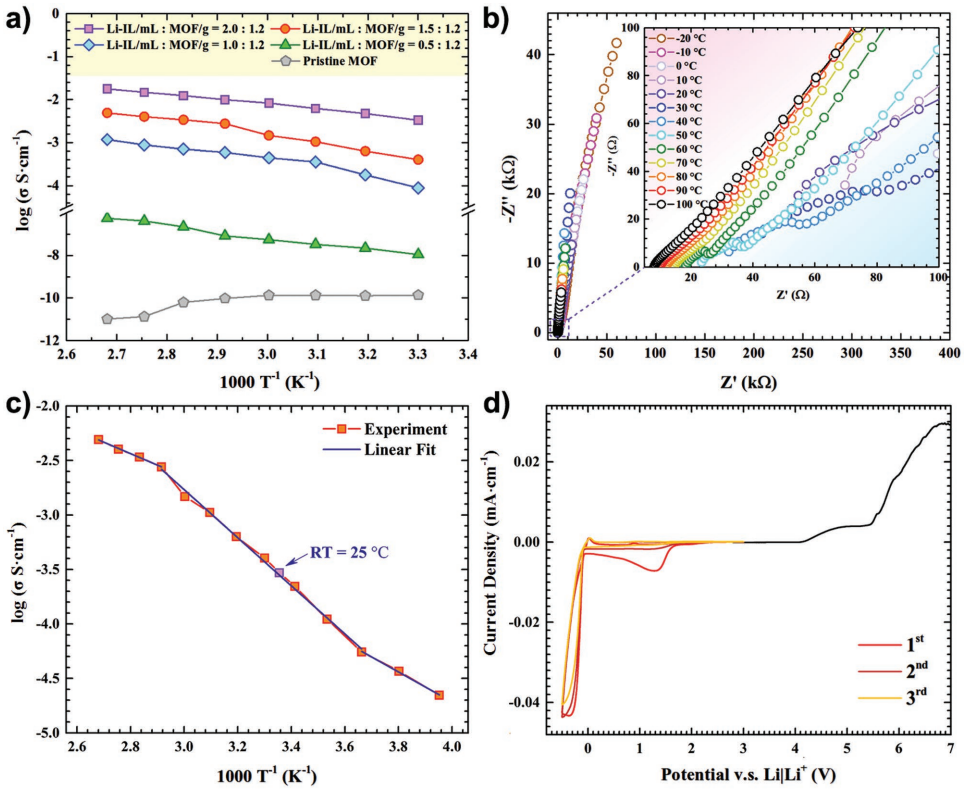

Figure 1. a) Arrhenius plots for the ionic conductivity of Li-IL@MOF SLEs with different Li-IL loading amount. b) EIS of Li-IL@MOF (1.5 mL: 1.2 g) at temperatures from –20 to 100 °C, inset: magnified high-frequency region, and c) corresponding Arrhenius plot of the ionic conductivity. d) CV (–0.5 to 3 V) for the first three cycles and LSV (3–7 V) profiles of Li|Li-IL@MOF|SS asymmetric cell under room temperature at a scan speed of 0.2 mV s^{-1}.

due to its big and semi-rigid organic ligands. The crystallinity of MOF could recover to some degree when the pellet was pulverized. The space group of MOF-525 is $Pm\bar{3}m$, so the location of the first diffraction peak ($2\theta = 4.56°$) of XRD represents the size of its unit cell and also the dimension of its pore. In detail, the first peak ({100}) of Li-IL@MOF pellet located at $2\theta = 4.56°$, and $d = \lambda/2\sin\theta = 19.38$ Å ($\lambda = 1.5418$ Å), which is equal to the reported cell parameter of MOF-525 ($a = b = c = 19.3930$ Å), demonstrating that the unit cells and the pores of the MOF host were actually intact after pressing. Furthermore, the morphology of Li-IL@MOF remained unchanged after pressing as proved by the cross-sectional SEM image of the SLE pellet (Figure S1b, Supporting Information), which also reveals a dense aggregation of the Li-IL@MOF nanocrystals. To further study the chemical stability of MOF with the Li-IL, the pulverized SLE was suspended into deionized water (1 wt%) for 12 h and then the supernatant liquid was collected for ultraviolet–visible (UV–vis) absorption test. As shown in Figure S6 (Supporting Information), using 1 ppm CuTPPCOONa (ligand of MOF) for reference, no absorption peak (at about 418 nm) corresponding to the ligand was detected, and the absorption peak at about 218 nm was caused by $[EMIM]^+$ ions, confirming a high chemical stability of MOF host against the Li-IL. The UV–vis result also provided additional evidence for the structural stability of MOF after pressing. Dense packing of the highly porous MOF nanocrystals with a high content of encapsulated Li-IL promise a high ionic conductivity.[20] Figure 1b shows the EIS of Li-IL@MOF at temperatures from –20 to 100 °C and Figure 1c shows the corresponding Arrhenius plot of ionic conductivity. High ionic conductivities of 2.2×10^{-5}, 3.0×10^{-4}, and 4.9×10^{-3} S cm^{-1} were observed at –20, 25 (room temperature), and 100 °C, respectively, which indicates stable battery electrochemical performance under a wide temperature range. Apparently, the ionic conductivity of Li-IL@MOF SLE relies on the bulk phase transport within Li-IL@MOF nanocrystals because it varied significantly with the Li-IL loading content, as shown in Figure 1a. However, only a conductive bulk phase is insufficient to explain the Li^+ transport mechanism between two adjacent MOF crystals. Also, the very small charge transfer resistances observed in the middle frequency region of Figure 1b demonstrated characteristics similar to liquid electrolytes[21,22] rather than solid ones.[7,23] As illustrated in Figure S7 (Supporting Information), when pressed into a dense aggregate, the MOF nanocrystals were packed together enabling the direct interfacial connection of the inner Li-IL through the highly porous open framework, that is, the interfaces were partially wetted by Li-IL at atomic level favoring Li^+ transport. The nanowetted interfaces existing in the Li-IL@MOF composite should also contribute a lot to the high ionic conductivity and the small charge transfer resistance of SLE pellet. Evidence for such nanowetted interfaces can be found by XPS, which offered abundant information about the surface (3–5 nm) of the Li-IL@MOF nanocrystals. As shown in Figure S4 (Supporting Information), strong F_{1s} and S_{1s} signals

belonging to the Li-IL were observed in the samples (Li-IL loadings of 0.5, 1.0, and 1.5 mL) with complete Li-IL impregnation, suggesting that Li-IL ions preferentially occupied the near-surface region of the MOF nanocrystals and the nanowetted interfacial phenomenon is observed for all Li-IL loading amount. Electrochemical window of the Li-IL@MOF SLE was further determined by the cyclic voltammetry (CV) and linear sweep voltammetry (LSV) profiles measured from a Li|Li-IL@MOF|SS asymmetric cell at room temperature, as illustrated in Figure 1d. A stable electrochemical window between 2 and 4.1 V was observed for the Li-IL@MOF SLE, almost identical to that of pristine Li-IL (Figure S8, Supporting Information), because the MOF host is stable against Li metal under a wide potential range.[15] In addition to the Li plating/stripping peaks, one small reduction peak located at about 1.3 V in the first several cycles of CV was observed, and it could be attributed to the $Cu^{2+} \rightarrow Cu^{+}$ reaction of MOF host. To prove this, we scanned the Li asymmetric cell of Li-IL@MOF to 0 V by CV test and then disassembled the cell to perform XPS on the material. Cu^{+} XPS peak at 932 eV[24,25] was detected, and it could not be found in the pristine Li-IL@MOF, as shown in Figure S9 (Supporting Information). The Li^{+} transference number (t_{Li+}) of Li-IL@MOF was measured using a Li|Li-IL@MOF|Li symmetric cell by Evans method[26] with a constant polarization potential of 10 mV at room temperature. The t_{Li+} of pristine Li-IL was only 0.14 (Figure S10a, Supporting Information) because the majority of the ionic conductive species in Li-IL are $[EMIM]^{+}$ and $[TFSI]^{-}$ rather than Li^{+}. A significantly increased t_{Li+} (0.36) was observed for Li-IL@MOF SLE as shown in Figure S10b (Supporting Information), which we speculate was caused by the confinement of the $[EMIM]^{+}$ and $[TFSI]^{-}$ ions by the MOF host.[27] The pores of the MOF are uniform with an aperture of about 12 × 7 Å, which is comparable to the sizes of IL ions (7.9 and 7.6 Å, respectively). The mobility of $[EMIM]^{+}$ and $[TFSI]^{-}$ ions were limited in MOF lattice while the movement of Li^{+} ions was less affected due to their small size (0.76 Å), resulting in an increased t_{Li+} of 0.36.

The direct current (DC) Li plating/stripping experiment was carried out to evaluate the impedance and Li-ion transport capability across the Li-IL@MOF SLE and Li metal interface. **Figure 2**a shows the time-dependent voltage profile of the Li|Li-IL@MOF|Li nonblocking cell under current densities of 0.05 and 0.2 mA cm^{-2}. The cell was run for 1 h with each cycle at room temperature. Small polarization voltages of ±40 and ±70 mV were observed for 0.05 and 0.2 mA cm^{-2}, respectively, indicating low interfacial impedance between the Li-IL@MOF SLE and the Li metal. Moreover, the voltage profile in each cycle was quite smooth and remained stable over 1000 h (1000 cycles), which represented a stable interface between the Li-IL@MOF SLE and the Li metal during cycling. As a comparison, cycling performance of a Li symmetric cell with glass fiber separator and pristine Li-IL electrolyte was tested in parallel. As shown in

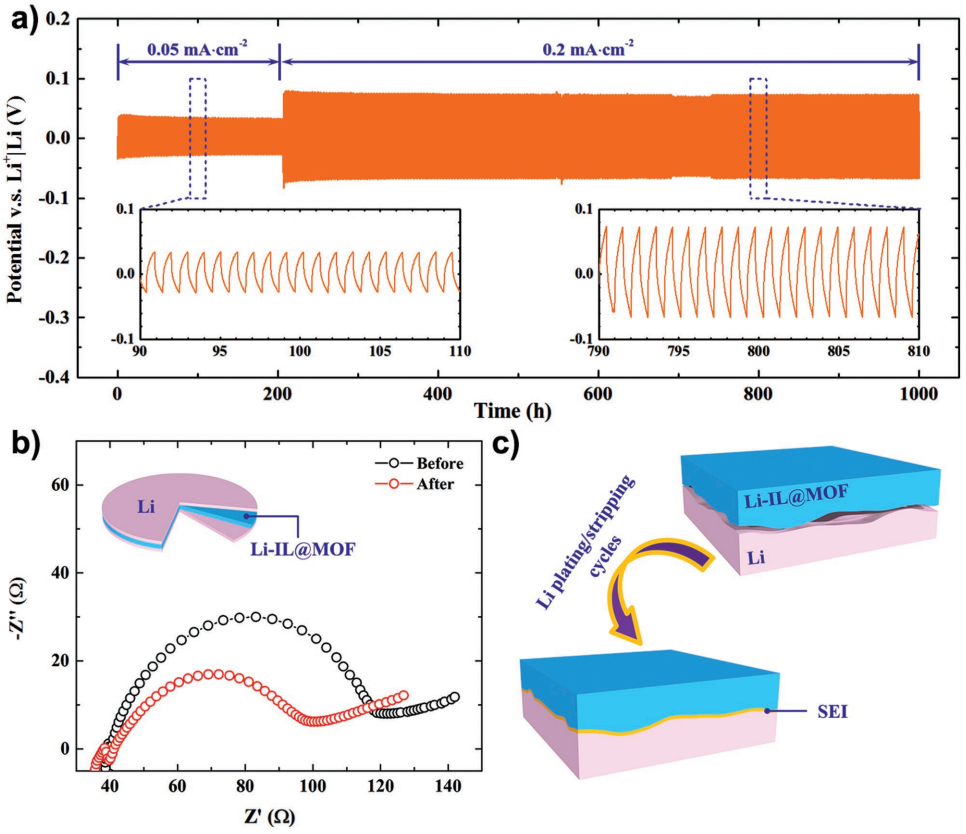

Figure 2. a) Voltage profiles for the Li|Li-IL@MOF|Li symmetric cell at current densities of 0.05 and 0.2 mA cm^{-2}. b) EIS of the Li|Li-IL@MOF|Li symmetric cell before and after the Li-plating/stripping cycles. c) Schematic illustration for the improved interfacial contact after Li-plating/stripping cycles.

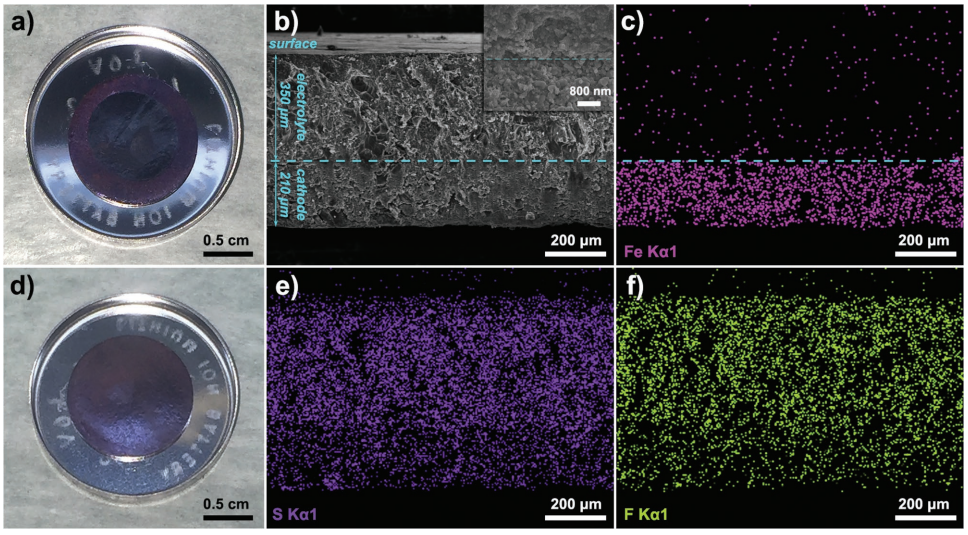

Figure 3. Photos of the a) cathode and d) electrolyte layers. b) SEM morphology for the cross section of the double-layer structure (the inset shows the interface between the two layers at a higher magnification) and c,e,f) corresponding EDS elemental mappings.

Figure S11 (Supporting Information), the polarization suddenly increased after cycling for about 450 h, and the cell became short-circuited near 640 h, which demonstrated inferior performance to the SLE Li symmetric cell. The improvements on the interfacial stability and compatibility of Li-IL@MOF SLE have some connections with the increased t_{Li+} of the electrolyte, as previously explained by Wang and co-workers.[27] EIS Nyquist plots of the Li|Li-IL@MOF|Li cell before and after Li plating/stripping experiment were compared, as shown in Figure 2b. The total resistance of the cell is about 130 Ω before cycling and it became smaller (120 Ω) after the cycling process. To clarify this, morphologies of the Li|Li-IL@MOF interface were further investigated by SEM. As shown in Figure S1c (Supporting Information), before cycling, gaps were found between the Li metal and the Li-IL@MOF layer due to the roughness and mismatching of the two surfaces. However, these gaps were filled after the Li plating/stripping cycles, forming a seamlessly connected interface (Figure S1d, Supporting Information) with reduced resistance. We found that the original gaps were actually filled up by a growth-inhibited "Li dendrite" layer. As shown in Figure S12 (Supporting Information), after Li platting/stripping cycles, the surface of the Li metal reveals a smooth and dense morphology. Instead of vertical Li dendrites, many tiled pancake-like nanostructures can be observed at a high magnification (inset of Figure S12, Supporting Information), for which we believe the uniform Li deposition[28] induced by nanowetted interfaces and good mechanical stability[29] of the Li-IL@MOF SLE layer should be responsible. Thus, the good compatibility of Li-IL@MOF SLE with Li metal, along with the small interfacial resistance between them can be well explained. Such interfacial mechanism is schematically illustrated in Figure 2c. Besides the long-term Li plating/stripping cycling, Li-IL@MOF SLE was also cycled in depth to test its reliability in a high energy density battery system. As shown in Figure S13 (Supporting Information), the current density was kept at 0.2 mA cm^{-2} for 2 d with each cycle. Then a large Li deposition amount of 4.8 mAh cm^{-2} was achieved for each half cycle. The voltage plateau became stabilized at about ±0.12 V and the total resistance was nearly unchanged after cycling, demonstrating a high electrochemical stability of the interface between the SLE and the Li anode even under large Li plating/stripping amounts.

The advantage of our Li-IL@MOF SLE was further evaluated in a Li|LFP rechargeable solid-state battery system. Commercially available $LiFePO_4$ was mixed with Li-IL@MOF and acetylene black to form the cathode, and the mixture was pressed sequentially with additional Li-IL@MOF electrolyte into a double-layered structure, as shown in **Figure 3**a,d. Charge/discharge behaviors of the electrodes with different cathode combinations were first studied to determine a reasonable LFP: Li-IL@MOF: C composition. The total loading of active LFP was fixed as high as 25 mg cm^{-2}. As displayed in Figure S14 (Supporting Information), discharge capacities of about 90, 128, 145, and 147 mAh g^{-1} were observed in the samples with LFP:Li-IL@MOF:C ratios of 5:1:2, 5:3:2, 5:5:2, and 5:7:2 (by weight), respectively, and the overpotential decreased with the Li-IL@MOF content growing. Considering maximizing the capacity and ensuring acceptable active content in electrode, the cathode composition of 5:5:2 was used in the following tests. Figure 3b demonstrates the SEM morphology for the cross section of such cathode|SLE bilayer pellet. In combination with the corresponding energy-dispersive spectrometer (EDS) elemental mappings (Figure 3c,e,f), a 210 μm cathode layer and a 350 μm electrolyte layer can be clearly distinguished. These two layers are seamlessly laminated as demonstrated in Figure 3b. In the cathode layer, the LFP grains are homogenously wrapped with conductive carbon and Li-IL@MOF SLE nanocrystals to form a dense 3D-connected structure (inset of Figure 3b), indicating good conductivity for both electrons and ions. Usually increasing the thickness of the cathode layer will dramatically increase the total resistance of batteries.[5] However, our Li|Li-IL@MOF|LFP SSB with such a thick cathode had a total resistance of only about 410 Ω before cycling (Figure S15, Supporting Information). The low resistance can be explained by the unique nanowetted interfacial mechanism

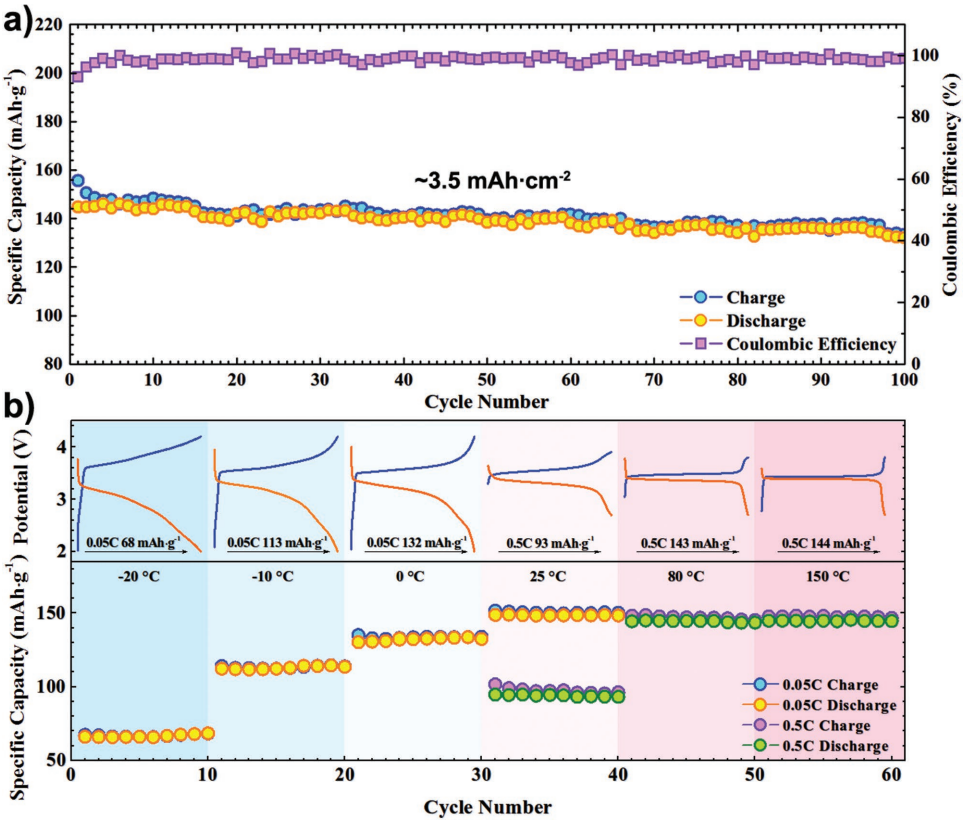

Figure 4. a) Cycling performance and Coulombic efficiency of the Li|Li-IL@MOF|LFP SSB with 0.1 C charge/discharge rate at room temperature. b) Temperature-dependent cyclability of the Li|Li-IL@MOF|LFP SSB with corresponding charge/discharge curves.

of Li-IL@MOF, which enhanced the Li^+ ions transport kinetics across the interfaces between the LFP and the SLE, and created a fast 3D-connnected Li^+ pathway throughout the cathode, as illustrated in Figure S7 (Supporting Information), ensuring excellent battery performance even with very high active loading of 25 mg cm^{-2} and a total cathode thickness of 210 µm. The wetting ability of Li-IL@MOF SLE on the LFP cathode and Li anode was further proved by EDS mappings and XPS. As shown in Figure S16 (Supporting Information), after a freshly prepared coin cell (not cycled) being disassembled, S belonging to Li-IL was detected on both surfaces of the cathode (prepared by coating method with polyvinylidene fluoride (PVDF) binder) and the Li anode without MOF (Zr or Cu) residues, which suggested that the surfaces of the electrodes can be wetted by Li-IL through contacting with Li-IL@MOF SLE. Charge/discharge cycling performance of the SSB at 0.1 C (1 C = 170 mA g^{-1}) rate under room temperature is shown in **Figure 4**a. An initial discharge capacity of 145 mAh g^{-1} was observed, and it slightly decreased to 132 mAh g^{-1} after 100 cycles (0.9‰ $cycle^{-1}$), and the total resistance of the cell increased to about 550 Ω with it. After cycling, the cell in the discharged state was disassembled and the interface between SLE and Li was studied by SEM and EDS. As shown in Figure S17 (Supporting Information), an SEI layer was found on the Li anode according to the EDS mappings. SEM morphology also suggested that after long-term cycling the SLE layer still maintained good contact with the Li anode. Figure S18 (Supporting Information) displays the thermogravimetric analysis (TGA) of the Li-IL@MOF SLE, showing a high degradation temperature over 300 °C. In view of the outstanding thermostability coupled with high ionic conductivity of our Li-IL@MOF SLE, we expected the cell could operate at both low and high temperatures. The Li|Li-IL@MOF|LFP SSBs were then cycled at selected temperatures of –20, –10, 0, 25, 80, and 150 °C, and the capacities with corresponding charge/discharge curves are shown in Figure 4b. Typically, an acceptable capacity of 67 mAh g^{-1} was obtained at a rate of 0.05 C at –20 °C while the polarization became extremely small at 80 and 150 °C, resulting in a reversible capacity of about 145 mAh g^{-1} at 0.5 C. Such a wide operating temperature range has been rarely reported in the previous solid-state battery systems, suggesting the advantage of our MOF-based SLE over the conventional SSE counterparts. In order to further increase the energy density and decrease the total resistance of SSB, the research about reducing the thickness of SLE layer is also carrying out and some preliminary results can be seen in the Supporting Information and Figure S19 (Supporting Information).

In this Communication, we demonstrated a novel solid-like electrolyte based on an ionic liquid impregnated metal–organic framework. Featuring a unique nanowetted interfacial mechanism with a dense morphology, the Li-IL@MOF SLE showed a high ionic conductivity of 3.0×10^{-4} S cm^{-1} at room temperature. It also exhibited good compatibility with both the active $LiFePO_4$ cathode with small interfacial resistance, and the Li metal anode as a result of uniform Li deposition and excellent mechanical stability. On top of that, with a super-high active loading of 25 mg cm^{-2} and a 210 µm thick cathode, high

electrochemical activity and good capacity retention over a wide temperature range (–20 to 150 °C) were observed in the Li|Li-IL@MOF|LFP SSB owing to the effective 3D-connected Li^+ transport network enabled by the high ionic conductivity and the nanowetted interfaces of Li-IL@MOF SLE. This work has provided a general and promising approach to the design of high energy density solid-state batteries. Not only with Li batteries, such strategy can be extended to other battery systems like K, Na, Mg, and Al batteries by changing the ion species in the ionic liquid, and these works are undergoing which will be reported in the near future.

Supporting Information

Supporting Information is available from the Wiley Online Library or from the author.

Acknowledgements

This work was financially supported by the National Materials Genome Project (2016YFB0700600), the National Natural Science Foundation of China (51672012), and Shenzhen Science and Technology Research Grant (Nos. JCYJ20150729111733470, JCYJ20151015162256516, and JCYJ20160531141048950).

Conflict of Interest

The authors declare no conflict of interest.

Keywords

ionic liquids, lithium batteries, metal–organic frameworks, nanowetted interfaces, solid-like electrolytes

Received: August 7, 2017
Revised: October 9, 2017
Published online:

[1] F. Wu, G. Tan, R. Chen, L. Li, J. Xiang, Y. Zheng, *Adv. Mater.* **2011**, *23*, 5081.
[2] J. Hassoun, B. Scrosati, *Adv. Mater.* **2010**, *22*, 5198.
[3] R. Chen, W. Qu, X. Guo, L. Li, F. Wu, *Mater. Horiz.* **2016**, *3*, 487.
[4] A. Manthiram, X. Yu, S. Wang, *Nat. Rev. Mater.* **2017**, *2*, 16103.
[5] K. Fu, Y. Gong, Y. Li, S. Xu, Y. Wen, L. Zhang, C. Wang, G. Pastel, J. Dai, B. Liu, H. Xie, Y. Yao, E. Wachsman, L. Hu, *Energy Environ. Sci.* **2017**, *10*, 1568.
[6] J. van den Broek, S. Afyon, J. L. M. Rupp, *Adv. Energy Mater.* **2016**, *6*, 1600736.
[7] K. Fu, Y. Gong, B. Liu, Y. Zhu, S. Xu, Y. Yao, W. Luo, C. Wang, S. D. Lacey, J. Dai, Y. Chen, Y. Mo, E. Wachsman, L. Hu, *Sci. Adv.* **2017**, *3*, 1601659.
[8] X. Yao, D. Liu, C. Wang, P. Long, G. Peng, Y. S. Hu, H. Li, L. Chen, X. Xu, *Nano Lett.* **2016**, *16*, 7148.
[9] B. M. Wiers, M. L. Foo, N. P. Balsara, J. R. Long, *J. Am. Chem. Soc.* **2011**, *133*, 14522.
[10] K. Fujie, R. Ikeda, K. Otsubo, T. Yamada, H. Kitagawa, *Chem. Mater.* **2015**, *27*, 7355.
[11] M. Watanabe, M. L. Thomas, S. Zhang, K. Ueno, T. Yasuda, K. Dokko, *Chem. Rev.* **2017**, *117*, 7190.
[12] M. Armand, F. Endres, D. R. MacFarlane, H. Ohno, B. Scrosati, *Nat. Mater.* **2009**, *8*, 621.
[13] C. Largeot, C. Portet, J. Chmiola, P. L. Taberna, Y. Gogotsi, P. Simon, *J. Am. Chem. Soc.* **2008**, *130*, 2730.
[14] W. Morris, B. Volosskiy, S. Demir, F. Gándara, P. L. McGrier, H. Furukawa, D. Cascio, J. F. Stoddart, O. M. Yaghi, *Inorg. Chem.* **2012**, *51*, 6443.
[15] Z. Wang, B. Wang, Y. Yang, Y. Cui, Z. Wang, B. Chen, G. Qian, *ACS Appl. Mater. Interfaces* **2015**, *7*, 20999.
[16] K. Fujie, T. Yamada, R. Ikeda, H. Kitagawa, *Angew. Chem., Int. Ed.* **2014**, *53*, 11302.
[17] S. Seki, Y. Kobayashi, H. Miyashiro, Y. Ohno, A. Usami, Y. Mita, N. Kihira, M. Watanabe, N. Terada, *J. Phys. Chem. B* **2006**, *110*, 10228.
[18] K. W. Chapman, G. J. Halder, P. J. Chupas, *J. Am. Chem. Soc.* **2008**, *130*, 10524.
[19] S. A. Moggach, T. D. Bennett, A. K. Cheetham, *Angew. Chem., Int. Ed.* **2009**, *48*, 7087.
[20] X. Han, Y. Gong, K. Fu, X. He, G. T. Hitz, J. Dai, A. Pearse, B. Liu, H. Wang, G. Rubloff, Y. Mo, V. Thangadurai, E. D. Wachsman, L. Hu, *Nat. Mater.* **2017**, *16*, 572.
[21] J. Ping, Y. Wang, K. Fan, W. Tang, J. Wu, Y. Ying, *J. Mater. Chem. B* **2013**, *1*, 4781.
[22] X. Peng, H. Liu, Q. Yin, J. Wu, P. Chen, G. Zhang, G. Liu, C. Wu, Y. Xie, *Nat. Commun.* **2016**, *7*, 11782.
[23] X. Liu, J. Tan, J. Fu, R. Yuan, H. Wen, C. Zhang, *ACS Appl. Mater. Interfaces* **2017**, *9*, 11696.
[24] P. Pallavicini, G. Dacarro, P. Grisoli, C. Mangano, M. Patrini, F. Rigoni, L. Sangaletti, A. Taglietti, *Dalton Trans.* **2013**, *42*, 4552.
[25] H. Wu, H. Li, X. Zhao, Q. Liu, J. Wang, J. Xiao, S. Xie, R. Si, F. Yang, S. Miao, X. Guo, G. Wang, X. Bao, *Energy Environ. Sci.* **2016**, *9*, 3736.
[26] J. Evans, C. A. Vincent, P. G. Bruce, *Polymer* **1987**, *28*, 2324.
[27] W. Liu, Y. Mi, Z. Weng, Y. Zhong, Z. Wu, H. Wang, *Chem. Sci.* **2017**, *8*, 4285.
[28] R. Miao, J. Yang, Z. Xu, J. Wang, Y. Nuli, L. Sun, *Sci. Rep.* **2016**, *6*, 21771.
[29] X. Yao, N. Huang, F. Han, Q. Zhang, H. Wan, J. P. Mwizerwa, C. Wang, X. Xu, *Adv. Energy Mater.* **2017**, *7*, 1602923.

